Bulletin of the Seismological Society of America, Vol. 95, No. 2, pp. 592–604, April 2005, doi: 10.1785/0120040099

Local and Duration Magnitudes in Northwestern Italy, and Seismic Moment Versus Magnitude Relationships

by D. Bindi, D. Spallarossa, C. Eva, and M. Cattaneo

Abstract In the present work, we develop some local magnitude scales for northwestern Italy based on vertical short-period records. This study is motivated by the possibility of applying the computed scales to an instrumental catalog of more than 25,000 local earthquakes, as this region has been continuously monitored by 12 short-period vertical-component (1C) stations since the mid-1980s. Furthermore, a digital network of three-component (3C) broadband or 5 second sensors has monitored northwestern Italy since 1996. Today, a significant number of earthquakes have been simultaneously recorded by both networks, allowing the calibration of the 1C local scale by using magnitudes computed according to a scale derived for the 3C digital network. Moreover, because station Sant' Anna di Valdieri houses both a 3C (code STV2) and 1C (code STV) sensors, the magnitude scales for the two networks can be developed using the same reference station. The magnitude scale $M_L = \log A + \log(R/100) + 0.0054(R - 100) + 3 - S$ is derived for the 3C digital network with the requirement that the correction S of station STV2 is zero. This scale is based on 10,057 maximum amplitudes (2822 earthquakes) computed from horizontal synthesized Wood-Anderson seismograms, in the hypocentral distance 10 to 310 km and in the range $0 \leq M_L \leq 5$. With respect to an carlier magnitude scale derived for the 3C network constraining the sum of all the station corrections to zero, the magnitudes predicted by the previous equations show an average bias of (-0.2 ± 0.1), which can be ascribed to the different constraint applied to the station corrections. The magnitudes predicted by the scale for the 3C network are used to calibrate magnitude scales based on either total duration or maximum amplitude from synthesized Wood-Anderson seismograms computed for each short-period vertical recording. The magnitude scale obtained considering maximum amplitudes from vertical short-period recordings is $M_L = \log A + \log(R/100) + 0.0041\ (R - 100) + 3 - S'$. The reliability of the obtained magnitude scales is assessed using 827 earthquakes different from those we considered in the regression analysis. Finally, the following seismic moment versus local magnitude relations are valid in the western Alps in the range $0 < M_L < 4.5$:

$$\log M_0 = (0.92 \pm 0.01)\, M_L^{3C} + (17.38 \pm 0.08)$$
$$\log M_0 = (0.95 \pm 0.01)\, M_L^{1C} + (17.36 \pm 0.01)$$

where M_L^{3C} is the local magnitude computed starting from the horizontal component of broadband (flat frequency response, from 0.033 to 50 Hz) or semibroadband (flat frequency response, from 0.2 to 40 Hz) sensors and M_L^{1C} is the magnitude computed starting from the vertical short-period recordings.

Introduction

Northwestern Italy is characterized by small to moderate seismicity ($M_L < 3$), and about two earthquakes of magnitude greater than 4.5 are expected each year (Spallarossa *et al.*, 2002). The recent largest earthquakes occurred on 21 August 2000 (Asti, M_L 4.8), on 18 July 2001 (Asti, M_L 4.6), and on 11 April 2003 (Novi Ligure, M_L 4.8). Seismogenic

structures able to generate a damaging earthquake are also present in this area. For example, the 1887, M_s 6.4 Bussana earthquake (Capponi *et al.*, 1985) that occurred in western Liguria, and the 1920, M_s 6.5 Lunigiana-Garfagnana earthquake (Ferrari *et al.*, 1985) that occurred in the northern Apennines caused significant damage and casualities. Since 1982, the RSNI/RSGL (Regional Seismic network of northwestern Italy, formerly the IGG network) has monitored seismicity in the western Alps and in the Ligurian sea and, since 1998, in the northern Apennines (Cattaneo and Augliera, 1990; Solarino *et al.*, 1997; Cattaneo *et al.*, 1999; Eva *et al.*, 2001; Solarino *et al.*, 2002). Furthermore, the northwestern Alps are contained in the area monitored by several seismological observatories (Laboratoire de Detection et de Geophysique [LDG/CEA], Bruyeres-le-Chatel, Frances; Swiss Seismological Service [SSS], Zurich, Switzerland; Laboratoire de Geophysique Interne et Tectonophysique [SISMALP], Grenoble, France; Reseau National de Surveillance Sismique [ReNaSS], Strasburg, France; Instituto Nazionale di Geofisica e Vulcanologia [INGV], Rome, Italy). To exploit the possibility of merging the catalog provided by the different networks, it is necessary to avoid inconsistencies in the method adopted to compute the considered parameters and to clearly state how the shared quantities were computed. An example is the magnitude, which is the parameter usually adopted for first-cut reconnaissance analysis of earthquake data for various geophysical and engineering investigations (Kanamori, 1983). Moreover, in general, magnitude is the only information about the size of the earthquake that spreads to the nonscientific community. Furthermore, magnitude catalogs are often subject of statistical analysis aimed at evaluating the seismic activity and at assessing the hazard of the considered area.

Several magnitude scales can be determined, based on amplitude measurements of different seismic phases or on the total signal duration. As pointed out in the *IASPEI New Manual of Seismological Observatory* (Bormann, 2002, p. 18), "there is no single number parameter available which could serve as a good estimate of earthquake size in all its different aspects." The local magnitude M_L (Richter, 1935, 1958) from actual or synthesized Wood-Anderson amplitude (Uhrhammer and Collins, 1990) is a good measure of earthquake size in terms of energy release and a good measure to specify seismic hazard. The major limitation to its applicability is the saturation that takes place for strong earthquakes, leading M_L to never exceed 7 (Kanamori, 1983, figure 4). The moment magnitude M_W, being proportional to the static average displacement and to the area of the fault, provides a measure of the total deformation in the source region and does not saturate for large earthquakes. In many seismological observatories that managed analog seismic networks characterized by short-period and low-dynamic equipment, magnitude scales based on total signal duration were developed. The magnitudes M_D reported in the RSNI bulletin (www.dipteris.unige.it/geofisica) are determined from the total signal duration visually estimated considering recordings from one-component, short-period stations. For each station, a M_D scale was calibrated in the early 1980s by using the magnitude reported in the LDG network bulletin, with no distance correction (Cattaneo *et al.*, 1981). More than 20 years of seismological observations in the western Alps demonstrated the reliability and stability of this duration scale in the magnitude range from 2 to 4 M_D, whereas, as shown in a work by Spallarossa *et al.* (2002, hereafter referred to as SP-02), this scale overestimates magnitudes below M_L 1.5 and underestimates magnitudes greater than 4. The overall goal of this study is the development of a reliable magnitude scale based on maximum amplitude from vertical short-period records that will allow us to compute a homogeneous magnitude catalog suitable for seismotectonic and hazard studies. SP-02 calibrated a local magnitude scale for the 3C network from synthesized Wood-Anderson seismograms, constraining the sum of all the station corrections to zero. To have the same reference for both the 3C and the short-period networks, a new 3C magnitude calibration is performed by imposing a different constraint over the station corrections. In particular, as station Sant'Anna di Valdieri houses both a 3C and a 1C sensor (code STV and STV2 for the 1C and 3C sensors, respectively), new coefficients for the M_L scale from 3C recordings are computed by setting to zero the station correction of STV2 alone. Then, regression analyses are carried out to derive new magnitude scales, based on duration and amplitude measurements from short-period instruments. Finally, exploiting an available dataset of seismic moment M_o (Morasca *et al.*, 2005), a comparison between M_L and log M_o is discussed.

Network and Data

The RSNI-Regional Seismic network of northwestern Italy arises from the integration of a regional network of telemetered short-period stations (formerly, IGG network) with a network of digital stations equipped with three-component (3C) sensors (Table 1). Signals from the 12 one-component (1C) short-period stations are transmitted by frequency modulation via telephone line to the Data-Processing Centre in Genoa, managed by DipTeRis (Dipartimento per lo studio del Territorio e delle sue Risorse). The transmission introduces a dynamic range limitation (about 66 dB) and a bandwidth reduction (0.2 to 25 Hz). At the Data-Processing Centre, signals are continuously digitized by a high-dynamic system and radio-synchronized to a DCF (German long wave signal Frankfurt) time signal. The 18 digital 3C stations are equipped with either Lennartz LE3D-5s sensors (flat frequency response from 0.2 to 40 Hz) or Guralp CMG40 sensors (flat frequency response from 0.033 to 50 Hz). The acquisition is performed by a dial-up LennartzMars88 MC system provided with a 20-bit A/D converter. Table 1 presents the main characteristics of the stations used in this work. Figure 1 shows the station locations and the local earthquakes recorded from 1996 to 2003. A detailed description

Table 1
Stations Used in This Study

Code	Latitude	Longitude	Height (km)	Sensor Type	Since (mm/yyyy)
BACM	44N16.70	10E04.33	0.49	Lennartz LE3D-5s (3C)	11/1998
CODM	44N23.45	09E51.00	0.35	Lennartz LE3D-5s (3C)	03/1999
FENE	45N01.81	07E03.76	1.00	Guralp CMG3 (3C)	10/1996
GENL	44N24.34	08E58.18	0.08	Guralp CMG40 (3C)	01/1996
GRAM	44N29.48	10E0395	0.87	Lennartz LE3D-5s (3C)	04/1999
MAIM	43N54.85	10E29.49	0.20	Lennartz LE3D-5s (3C)	09/2000
MONE	44N04.77	07E45.30	1.32	Guralp CMG40 (3C)	02/1995
NEGI	43N50.86	07E42.23	0.64	Guralp CMG40 (3C)	03/1996
RONM	43N54.88	07E35.89	0.30	Guralp CMG3 (3C)	01/1999
RORM	44N52.88	07E35.89	0.30	Guralp CMG3 (3C)	03/2001
ROTM	44N50.96	08E21.16	0.22	Lennartz LE3D-5s (3C)	07/2001
SARM	44N11.05	10E24.06	1.04	Lennartz LE3D-5s (3C)	03/1998
SCUM	44N24.98	09E32.23	0.75	Lennartz LE3D-5s (3C)	11/1998
SESM	44N13.91	10E46.42	1.02	Lennartz LE3D-1s (3C)	07/2002
STV2	44N14.73	07E19.56	0.93	Guralp CMG40 (3C)	10/1996
TRAV	45N30.76	07E44.82	0.99	Guralp CMG40 (3C)	09/1996
VALM	44N20.94	10E14.83	0.79	Lennartz LE3D-5s (3C)	03/1999
VINM	44N08.47	10E0913	0.71	Lennartz LE3D-5s (3C)	10/1998
ROB	44N17.75	07E53.18	0.81	Geotech S13 (1C)	06/1985
BLB	44N50.11	07E15.80	0.58	Geotech S13 (1C)	05/1990
ENR	44N13.77	07E25.10	1.03	Geotech S13 (1C)	05/1989
FIN	44N12.49	08E12.53	0.60	Geotech S13 (1C)	06/1984
IMI	43N54.63	07E53.59	0.84	Geotech S13 (1C)	11/1983
LSD	45N27.57	07E08.06	2.28	Geotech S13 (1C)	10/1985
ORX	45N37.90	07E58.90	1.23	Kinemetrics SS1 (1C)	12/1984
PCP	44N32.48	08E32.71	0.77	Geotech S13 (1C)	03/1989
PZZ	44N30.41	07E06.9	1.43	Kinemetrics SS1 (1C)	06/1985
RRL	44N55.25	06E47.45	2.13	Kinemetrics SS1 (1C)	06/1985
RSP	45N08.89	07E15.92	1.28	Geotech S13 (1C)	06/1985
STV	44N14.73	07E19.56	0.93	Geotech S13 (1C)	12/1985

of the detection capabilities and location accuracy of the RSNI network can be found in Spallarossa *et al.* (2001).

In the present study, we selected earthquakes with epicenters inside the investigated region (Fig. 1), azimuthal gap less than 220 degrees, and statistical horizontal and vertical location errors (Lee and Lahr, 1975) less than 10 and 20 km, respectively. In all, 4832 earthquakes occurring from 1996 to 2003 are part of the analyzed dataset.

Ml Calibration Using Three-Component (3C) Recordings

Data recorded from 1999 to 2003 are used to compute a local magnitude scale using synthetic Wood-Anderson amplitudes obtained from the horizontal component of 3C recordings. We calibrate a M_L scale (Richter, 1935, 1958) following the Bakun and Joyner (1984) parametric approach:

$$M_L = \log A + n \log(R/100) + k(R - 100) + 3 - S, \quad (1)$$

where A is the observed maximum amplitude of the horizontal Wood-Anderson seismogram, n and k are attenuation coefficients, S is a station correction, and R is the hypocentral distance. The 1-mm amplitude constraint for a magnitude 3 recorded at distance $R = 100$ km is applied. If amplitudes from seismometers different from the Wood-Anderson are handled, it is a common practice (Uhrhammer and Collins, 1990) to compute synthetic Wood-Anderson seismograms by convolving the displacement corrected for instrumental response with the Wood-Anderson torsion seismograph response. We use $T_0 = 0.8$ sec, $h = 0.8$, and $V = 2800$ to describe the Wood-Anderson response, consistently with most of the local magnitude studies that adopted this value for the static magnification V instead of the correct value of 2080 (Uhrhammer and Collins, 1990). To avoid amplification of the noise at low frequency, the instrument correction and the Wood-Anderson convolution are performed in a frequency band for which the signal-to-noise ratio is greater than 5.

A local magnitude scale was calibrated for the 3C network by SP-02 using synthesized Wood-Anderson seismograms and constraining the sum of all the station corrections to zero. To have the same reference for both the 3C and the short-period networks, a new 3C magnitude calibration is performed by setting to zero the correction of station STV2 alone. The constraint applied to the station corrections introduces a dependence of the calibrated scale on the assumption

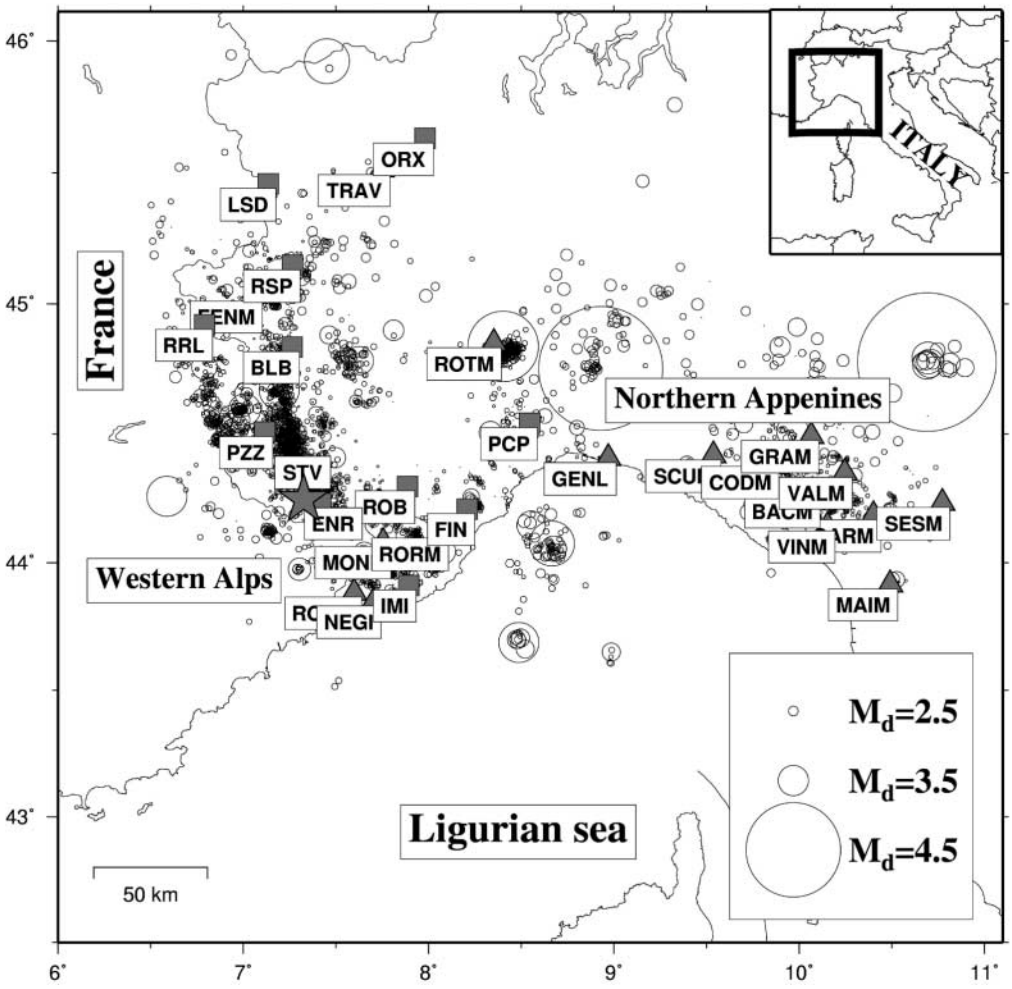

Figure 1. Seismicity recorded in the northwestern Alps and northern Apennines by the RSNI network from 1996 to 2003. Triangles and squares indicate three-component (3C) and one-component (1C) stations, respectively. Station STV/STV2 is indicated by a star. Duration magnitude is taken from RSNI weekly bulletins.

made about the reference station. Because the magnitude of an earthquake is generally computed as the average of the magnitudes estimated from the maximum amplitude observed at several stations, from equation (1) it follows:

$$M_L = \frac{1}{N}\sum_{i=1}^{N} M_L^i = \frac{1}{N}\sum_{i=1}^{N} (\log A^i + n \log(R^i/100) + k(R^i - 100) + 3) - \frac{1}{N}\sum_{i=1}^{N} S^i \quad (2)$$

where the index $i = 1, \ldots, N$ spans the stations that recorded the earthquake. Although the second term of the right hand side of equation (2) was set to zero in SP-02, it is different from zero in the present calibration. From equation (2) it follows that the average magnitudes computed in this study will differ from those computed from SP-02 by an offset equal to the second term of the right hand side, that is, the arithmetic mean of the station corrections estimated in this study.

The calibration is performed by considering 10,057 amplitudes from 2822 earthquakes recorded at 18 stations, in the range of distances from 10 to 310 km and following the same procedure described in SP-02. Only the earthquakes occurring from 1999 to 2003 are accounted for in this calibration. Figure 2 shows the locations of the earthquakes used to calibrate the scale, the relative path coverage, the distribution in distance of the recordings, and the histogram of the horizontal location errors. Because a trade-off between the geometrical spreading parameter n and the anelastic attenuation parameter k exists (Bakun and Joyner, 1984; Langston *et al.*, 1998), we perform the inversion constraining $n = 1$. The linear system is solved in a least-squares sense by applying the LSQR technique (algorithm for sparse linear equations and sparse least squares) (Paige and Saunders, 1982). The station corrections and the attenuation coefficient

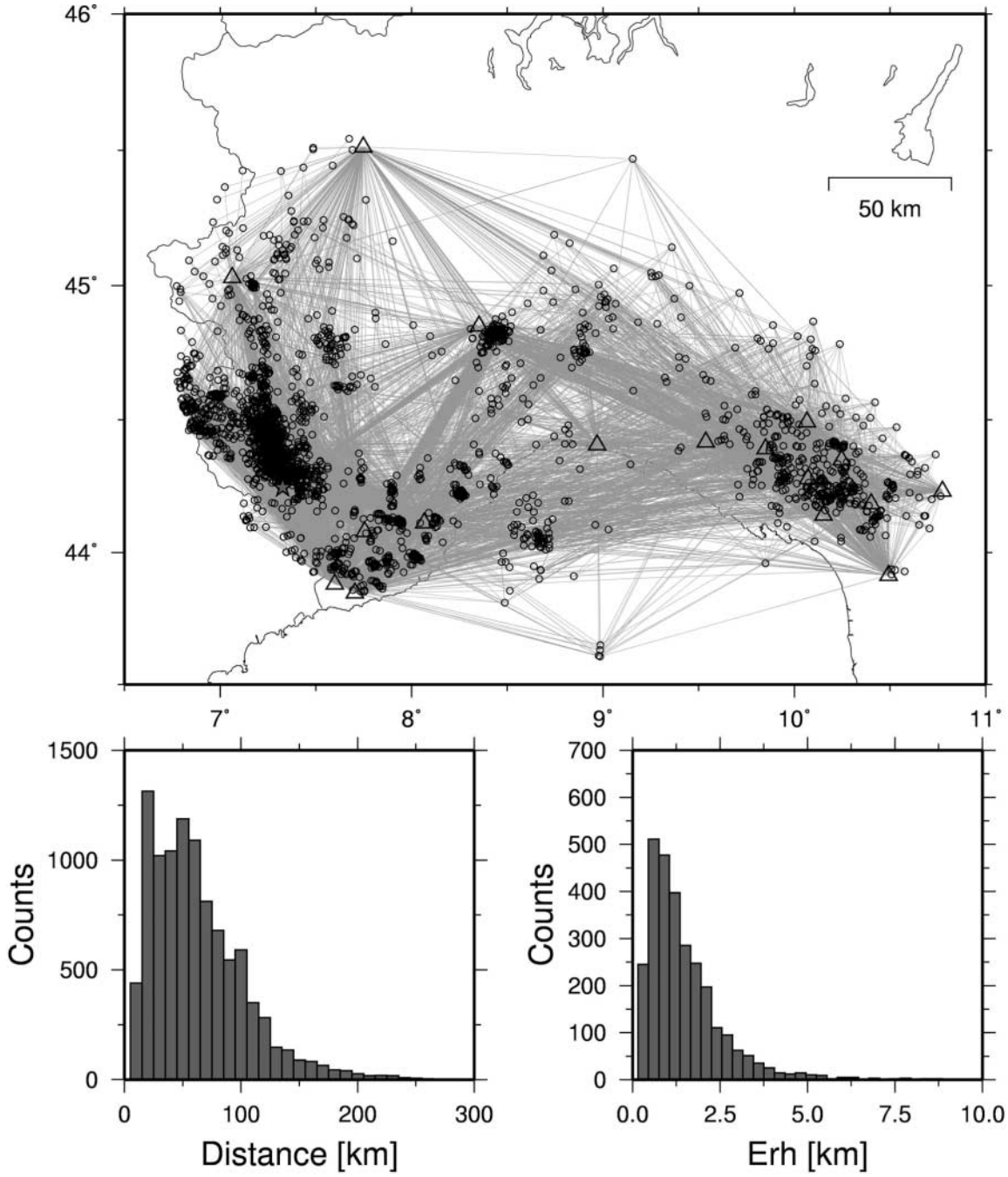

Figure 2. Ray paths between events (circles) and stations (triangles) used in the 3C local magnitude calibration and the histograms of the distance distribution (left bottom panel) and horizontal location error (right bottom panel).

k are estimated by computing the mean and the standard deviation of the distributions resulting from the inversion of 200 bootstrap replications of the original dataset (Efron, 1979; Spallarossa *et al.*, 2002; Baumbach *et al.*, 2003). The inversion yielded $k = (0.0054 \pm 0.0003)$. The station corrections (Table 2) vary in the range (-0.13 ± 0.06) to (0.57 ± 0.04), whereas the magnitudes are in the range 0 to 5. Figure 3 (left) shows the magnitudes computed in this study versus the magnitudes obtained by SP-02. Because the differences between the attenuation curves are negligible (Fig. 3, right), the average difference of (-0.2 ± 0.1) between the magnitudes computed in this study and those computed by SP-02 is in good agreement with the value 0.18 expected from equation (2) by using the station corrections listed in Table 2.

A peculiarity of the magnitude calibration scheme is the

Table 2
Number of Earthquakes (#) Used to Calibrate the M_L^{3C} Magnitude Scale and the Resulting Station Corrections S

Code	#	S	ΔS
STV2	1169	0	0.
MONE	1617	0.46 ± 0.02	0.43
RONM	200	0.38 ± 0.02	0.34
SARM	369	−0.01 ± 0.02	−0.02
VINM	317	0.25 ± 0.03	0.25
BACM	335	0.20 ± 0.03	0.19
SCUM	420	0.18 ± 0.03	0.17
GENL	173	0.02 ± 0.03	0.03
TRAV	237	0.10 ± 0.03	0.10
CODM	288	0.18 ± 0.03	0.20
GRAM	384	0.37 ± 0.02	0.35
VALM	261	0.44 ± 0.03	0.44
SESM	34	0.11 ± 0.07	0.06
ROTM	47	0.57 ± 0.04	0.57
MAIM	35	−0.13 ± 0.05	−0.15
NEGI	890	0.17 ± 0.02	0.13
FENM	94	−0.03 ± 0.04	−0.05
RORM	234	0.01 ± 0.03	0.02

ΔS is the difference, obtained by applying the inversion scheme of Uhrhammer *et al.* (1996) between each station correction and the correction for STV2.

non-uniqueness of the solution due to the trade-off between the magnitudes and the station corrections. To remove the trade-off, a constraint was applied to station corrections. To verify whether the constraint on STV2 was successful in removing the trade-off between M_L and S, the differential scheme proposed by Uhrhammer *et al.* (1996) is also applied. In this method, equations for the same earthquake are subtracted to eliminate the needed of determining M_L and S simultaneously, that is:

$$\begin{cases} \log A_1 = M_L - \log(R_1/100) - k(R_1 - 100) - 3 - S_1 \\ \log A_2 = M_L - \log(R_2/100) - k(R_2 - 100) - 3 - S_2 \\ \qquad\qquad \dots \end{cases} \quad (3)$$

where indexes 1 and 2 indicate two different recordings for the same earthquake. By subtracting the first two equations in (3), we obtain:

$$\begin{cases} \log(A_1/A_2 = -\log(R_1/R_2) - k(R_1 - R_2) - (S_1 - S_2) \\ \qquad\qquad \dots \end{cases} \quad (4)$$

Because the magnitudes do not appear in the linear system composed by equations similar to (4), an absolute calibration of the differences between the station corrections can be obtained. Anyway, for an absolute calibration of each station correction, the differential scheme requires the assumption of the correction of one reference station. Table 2 shows the differences between each station correction and the correction for STV2 as obtained by applying the differential inversion. Because the differences between the two calibration schemes are less than 0.05, we can conclude that the constraint applied to station STV2 avoided the trade-off between magnitudes and station corrections.

The computed local magnitudes (hereinafter, M_L^{3C}) are then used to calibrate both amplitude and duration magnitude scales for vertical recordings from short-period sensors, as discussed in the next sections.

Amplitude 1C Magnitude Scales

A magnitude scale based on synthetic Wood-Anderson amplitudes computed from vertical short-period (1C) recordings is also determined (hereinafter, M_L^{1C}). Reliable amplitude-frequency response of each short-period instrumentation system is not currently available. An empirical estimate of the transfer function is obtained comparing the waveforms of the same earthquake recorded by both short-period and broadband sensors installed at the same site. This reference site, indicated by a star in Figure 1, is equipped with both a telemetered short-period station (code STV) and a 3C broadband digital station (code STV2). The input vertical ground motion, which is assumed to be the same for both sensors, is evaluated correcting the vertical component of STV2 for its (known) instrument response. Then, the unknown transfer function of the whole acquisition chain (field package and transmission equipment) relevant to station STV is determined by deconvolving the input ground motion from the output recordings. The spectral deconvolution is performed over the range 0.4 to 25 Hz. Figure 4 depicts an example of 1C whole-chain transfer function retrieval: (a) the output of the STV acquisition chain; (b) the vertical component of STV2 after correction for instrumental response; (c) the estimated transfer function (time domain) of STV acquisition chain; (d) its amplitude Fourier spectrum (dotted line) and the result of a least-squares grid search applied to fit the amplitude spectrum using a pole-zero file (continuous line). This procedure is repeated for 10 earthquakes in the magnitude range 2 to 4, and the average transfer function is computed. This function is assumed to describe the system response of all the telemetered stations except for the gain value, which could differ from station to station. Amplitude noise analysis (not reported in this article) is performed to ensure that the gain value for each station is time independent from 1996 to 2003.

The synthetic maximum Wood-Anderson amplitudes derived from telemetered short-period network are used to calibrate an amplitude magnitude scale for each 1C station by using the following approach:

$$\begin{aligned} M &= \log(A/G) + n\log(R/100) + k(R - 100) - S + 3 \\ &= \log(A) + \log(R/100) + k(R - 100) - S' + 3, \end{aligned} \quad (5)$$

where M is the local magnitude value used to calibrate the scale, A is the maximum vertical synthetic Wood-Anderson amplitude, G is the unknown gain value, n and k are the attenuation parameters, R is the hypocentral distance, and S is the station correction. We assume $n = 1$ and we introduce

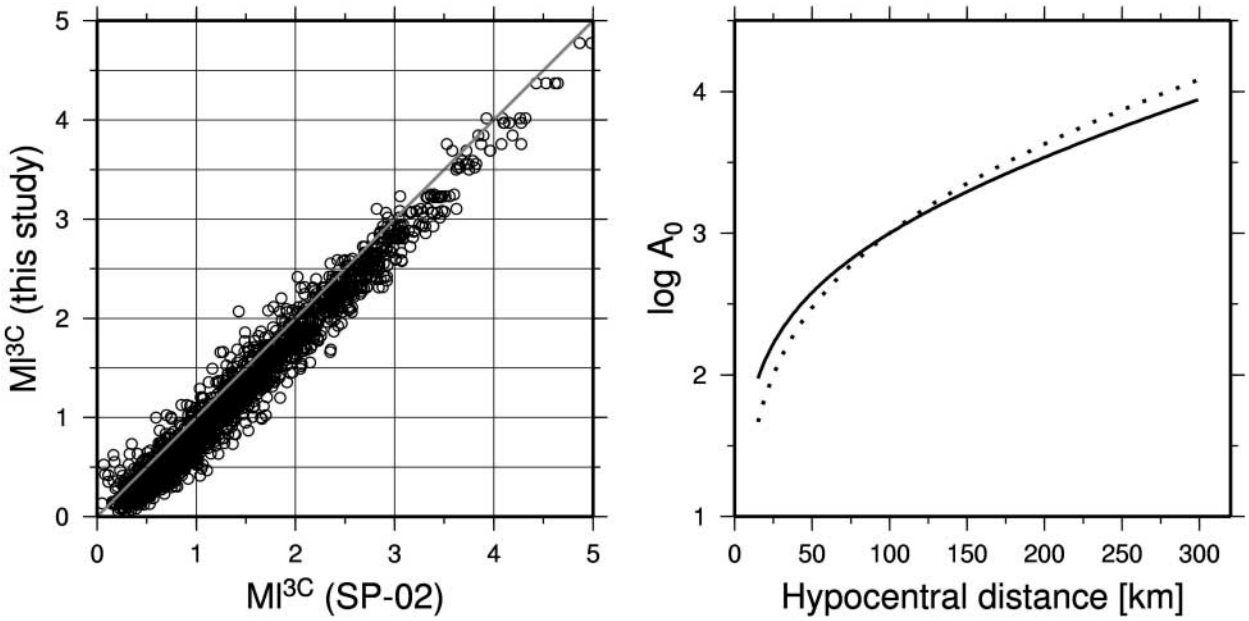

Figure 3. (Left) Local magnitudes estimated in this study versus Spallarossa *et al.* (2002). (Right). Attenuation function $\log A = n \log(R/100) + k(R - 100)$ for $n = 1$, $k = 0.0054$ (this study, black line) and $n = 1.144$, $k = 0.00476$ (Spallarossa *et al.*, 2002, dotted line).

$S' = S + \log(G)$, which is a station correction that accounts for both magnitude correction and gain value. Given a set of earthquakes having known local magnitude M, computed according to the M_L^{3C} scale, equation (5) is used to calibrate k and S' for the short-period network constraining the correction S' of station STV to zero. The calibration is performed considering 16,166 amplitudes from 2730 earthquakes recorded at 12 stations in the distance range from 10 to 310 km. The linear system is solved in a least-squares sense with the same method adopted for the calibration of the 3C scale. The obtained k is (0.0041 ± 0.0001), and the station corrections S' are shown in Table 3.

Duration Magnitude

We calibrated a magnitude scale based on signal duration of the form (Real and Teng 1973; Herrmann, 1975):

$$M_D = c_0 + c_1 R + c_2 \log \tau \qquad (6)$$

where τ is the particular duration used and R is the hypocentral distance. In the present work, the duration is defined as the interval between the onset of the first arrival and the point at which the signal-to-noise ratio is definitely less than 1.5. The signal-to-noise ratio is computed considering a pre-event window 2 sec wide, and τ is estimated based on seismograms filtered in the frequency band 1–12 Hz. The calibration is performed by considering 10,842 recordings from 2538 earthquakes recorded at 12 stations in the distance range from 10 to 310 km. Table 3 lists the c_0, c_1, and c_2 coefficients for all the stations. Small values for c_1 are found to be in agreement with a weak dependence of signal duration on distance.

Validation

Earthquakes recorded from 1996 to 1998 are used to validate the obtained magnitude relationships. Figure 5 shows the 1C magnitude residuals, that is, the difference between the station magnitude and the arithmetic mean of the station magnitudes for the same event (event magnitude) versus the hypocentral distance (center panels). The dependence on the event magnitude (left panels) and the histograms of the residuals (right panels) are shown as well. The results for the two selected stations in Figure 5 are representative of the results obtained for all the other stations. The residuals do not show any significant trend with distance, suggesting that the applied correction in term of k properly accounted for the attenuation characteristics in the area. The average residuals range from 0.001 (station BLB) to 0.04 (STV and ROB stations) and, in general, the standard deviation is close to 0.2.

Figure 6 shows the duration magnitude residuals versus duration (left frames) and distance (center frames). The histograms of residuals are shown as well (right frames). The average residual varies from 0.03 (STV) to 0.05 (BLB), and the standard deviation is 0.2. The residuals are nearly independent of distance, whereas they increase with decreasing duration over the short-duration range. In particular, for duration less than 20 sec ($\log \tau = 1.3$, vertical dotted lines in

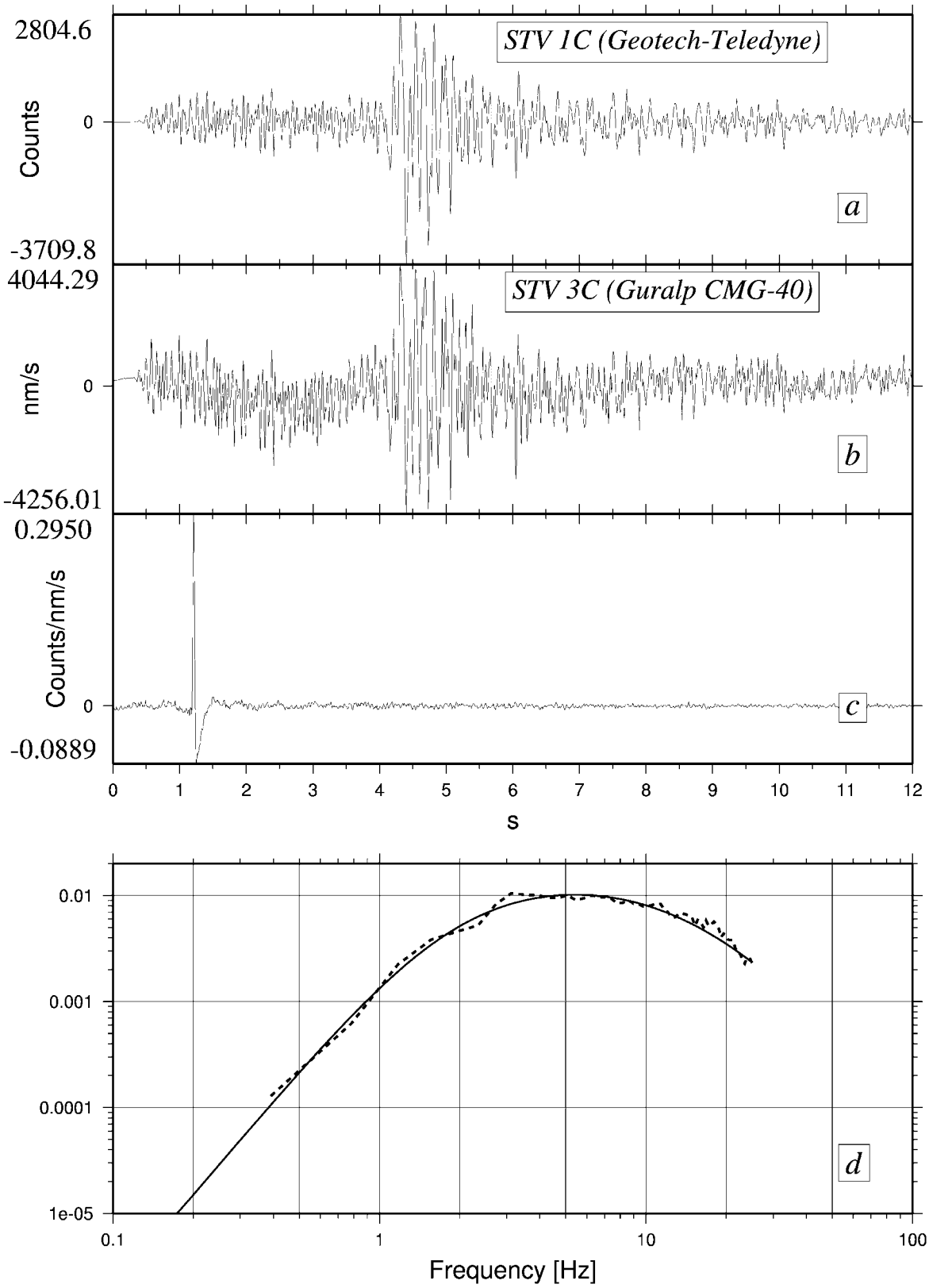

Figure 4. (a) Output of the STV acquisition chain (telemetered station equipped with a vertical short-period sensor). (b) Vertical component of STV2 (broadband sensor) after correction for instrumental response. (c) Estimated transfer function (time domain) of STV acquisition chain. (d) Amplitude Fourier spectrum of the STV transfer function (dotted line) and the result of a least-squares grid search applied to fit the amplitude spectrum using a pole-zero file (continuos line).

Table 3
Number of Earthquakes (#) Used to Calibrate the M_L^{1C} and M_D Magnitude Scales and the Obtained Regression Coefficients

		M_L^{1C}		M_D	
Code	#	S'	c_0	$c_1(\times 10^{-3})$	c_2
ROB	1578	−0.09 ± 0.01	−2.1 ± 0.1	4.9 ± 0.5	2.07 ± 0.07
PZZ	1789	0.27 ± 0.01	−2.1 ± 0.1	4.0 ± 0.4	1.97 ± 0.06
IMI	1323	0.07 ± 0.01	−2.0 ± 0.1	4.4 ± 0.5	2.01 ± 0.09
LSD	401	0.06 ± 0.02	−2.1 ± 0.4	4.0 ± 0.7	2.16 ± 0.09
RRL	617	−0.24 ± 0.01	−1.9 ± 0.2	3.0 ± 0.7	2.17 ± 0.09
ORX	232	−0.07 ± 0.02	−1.7 ± 0.4	5.7 ± 0.7	1.77 ± 0.09
FIN	1322	0.00 ± 0.01	−1.7 ± 0.1	4.3 ± 0.5	1.89 ± 0.08
PCP	922	−0.02 ± 0.01	−1.8 ± 0.1	2.8 ± 0.5	2.11 ± 0.08
ENR	1905	0.15 ± 0.01	−1.7 ± 0.1	4.0 ± 0.5	1.90 ± 0.07
BLB	1371	0.06 ± 0.01	−1.8 ± 0.1	4.6 ± 0.7	1.93 ± 0.08
RSP	746	−0.14 ± 0.01	−2.7 ± 0.2	2.8 ± 0.7	2.61 ± 0.07
STV	1611	0.	−1.8 ± 0.1	3.7 ± 0.5	1.97 ± 0.07

Fig. 6), the station magnitudes are overestimated, leading to an average residual of about 0.2. Then, the corrections for distance applied to duration magnitude are effective, whereas the corrections for duration are reliable only for duration longer than 20 sec which approximately corresponds to a magnitude greater than 1.

Figure 7 compares the local 3C magnitudes with the local magnitudes from short-period data, considering both the 1C amplitude and duration scales. The 3C and 1C scales (top panel) provide values in good agreement over the whole analyzed magnitude range. The distribution of the differences has a mean of 0.03 and a standard deviation of 0.20. The M_D and M_L^{3C} are consistent up to magnitude $M_L^{3C} = 3$. Beyond this value, the duration scale saturates, furnishing values not exceeding 3.5. In particular, the distribution of differences has mean values and standard deviations as follows: (-0.24 ± 0.25) for $M_L^{3C} < 1$; (-0.02 ± 0.23) for $1 \le M_L^{3C} \le 3$; (0.5 ± 0.4) for $M_L^{3C} > 3$. The computed duration magnitude scale can be considered reliable in the range 1 to 3.

Seismic Moment Magnitude Relationships

Regressions for seismic moment M_o versus local magnitude are also performed. The seismic moment of 344 earthquakes, ranging from 10^{17} to 10^{21} dyne cm, are taken from Morasca *et al.* (2005), who calibrated source spectra in the western Alps using the coda method developed by Mayeda *et al.* (2003). Moreover, using the coda-derived seismic moments and local magnitudes computed in agreement with SP-

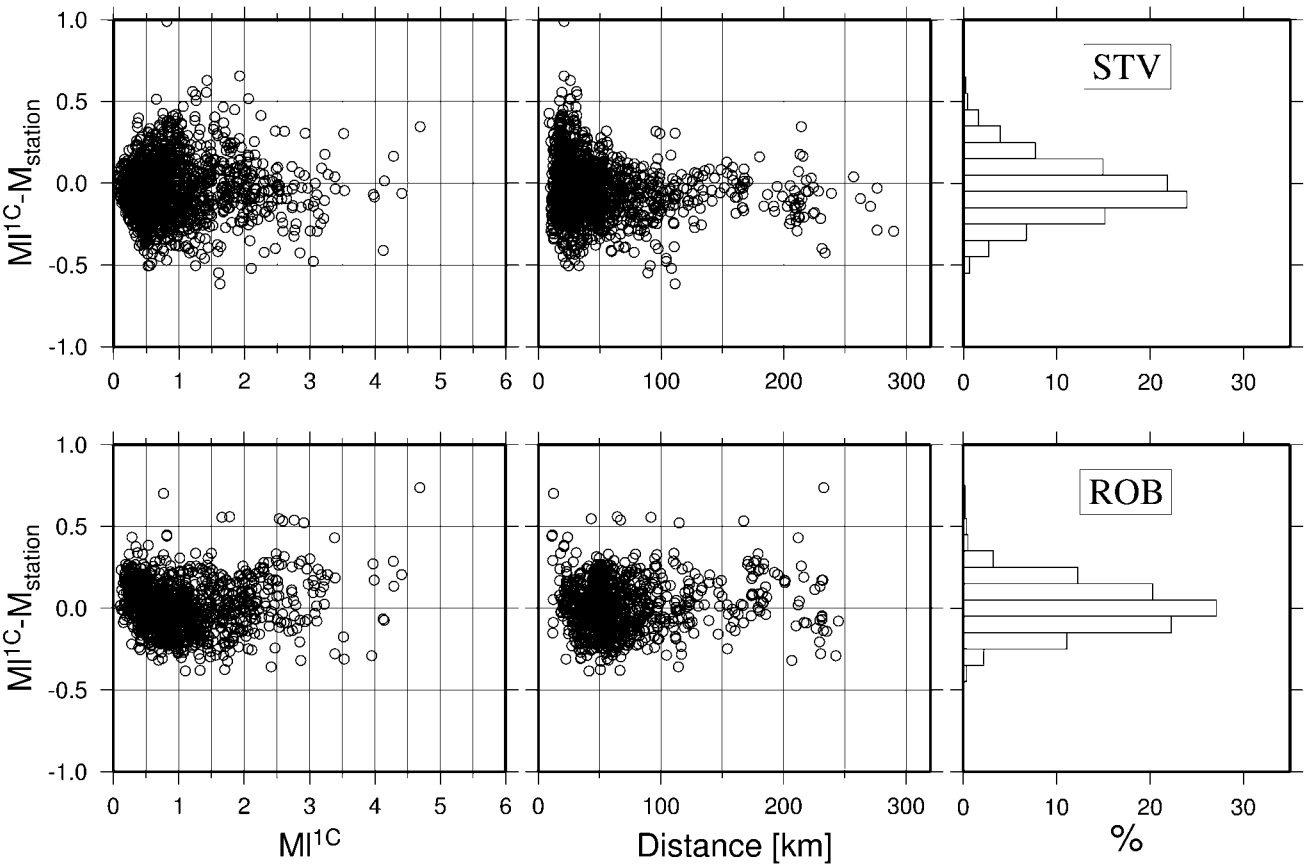

Figure 5. Examples for two stations of magnitude residuals for the amplitude short period scale (M_L^{1C}) versus event magnitude (left panels) and hypocentral distance (center panels). The histograms of the residuals are shown as well (right panels).

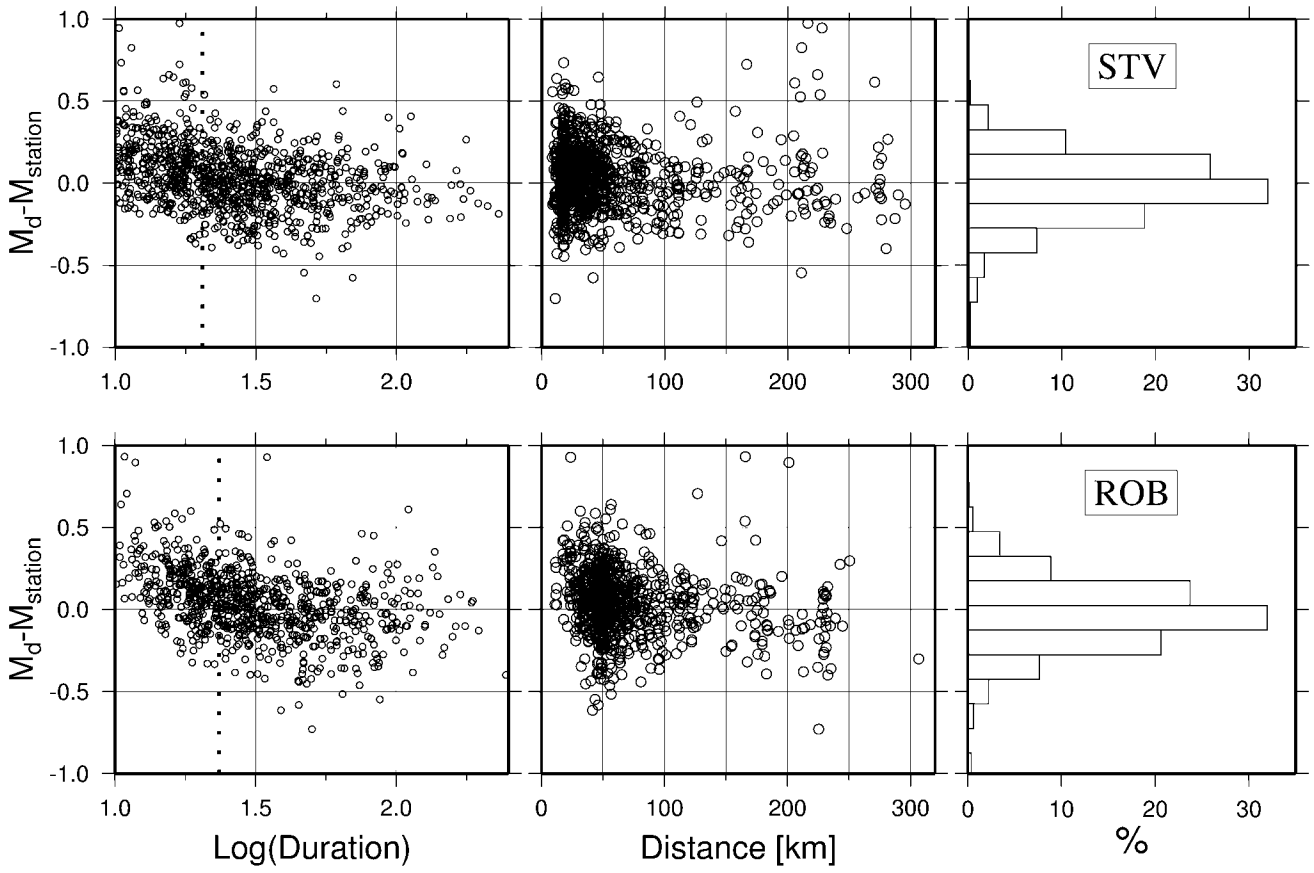

Figure 6. Examples for two stations of magnitude residuals for the duration scale (M_D) versus logarithm of duration (left panels) and distance (middle panels). The duration is measured in seconds. The histograms of the residuals (right panels) are shown as well. In the left panels, the vertical dotted lines at $\log \tau = 1.3$ indicate the assumed lower bound of validity of the magnitude duration scale.

02, they also calibrated an equivalent local magnitude scale that provides very stable single-station magnitude values. Most of the earthquakes we considered have seismic moments less than 10^{20} dyne cm, and only six events have higher seismic moments. Because all the considered seismic moments are relevant to earthquakes occurring in the western Alps, the derived relationships can be considered reliable only inside this area.

We carry out moment versus magnitude regression analysis considering both the M_L^{3C} and the M_L^{1C} scales. In general, when computed over a broad magnitude range, the relation $\log M_0$ versus magnitude shows a continuous positive curvature (Bakun, 1984; Hanks and Boore, 1984), that is, the linear model $\log M_0 = cM_L - d$ requires c values that increase with M_L. It follows that a quadratic term is needed to fit data ranging over a wide range with a single scaling relation (Hanks and Boore, 1984; Ben-Zion and Zhu, 2002). The need of a quadratic term was explained by Hanks and Boore (1984) as resulting from the complex interaction, in the frequency domain, between the Wood-Anderson response spectrum and an ω-square source model with constant stress drop, whereas Ben-Zion and Zhu (2002) suggested an alternative possible explanation based on the assumption that "the occurrence of increasingly larger events is associated with increasingly smoother stress field" (Ben-Zion and Zhu, 2002, p. F2).

Figure 8 shows $\log M_o$ against both M_L^{1C} and M_L^{3C}. Only the results obtained considering the linear model are shown, because the solutions for both the linear and quadratic relations produce the same root mean square of residuals (e.g., 0.14 in M_L^{3C}). This result was expected because the bulk of analyzed magnitudes is in the range of 0 to 2.5, and only nine earthquakes have a magnitude larger than 2.5. The best least-squares fits are:

$$\log M_0 = (0.95 \pm 0.01)\, M_L^{1C} + (17.36 \pm 0.01)$$
$$\log M_0 = (0.92 \pm 0.01)\, M_L^{3C} + (17.38 \pm 0.08)$$

For a magnitude less than 2.5, these relations are similar to the result found in the northeastern Alps (Granet and Hoang

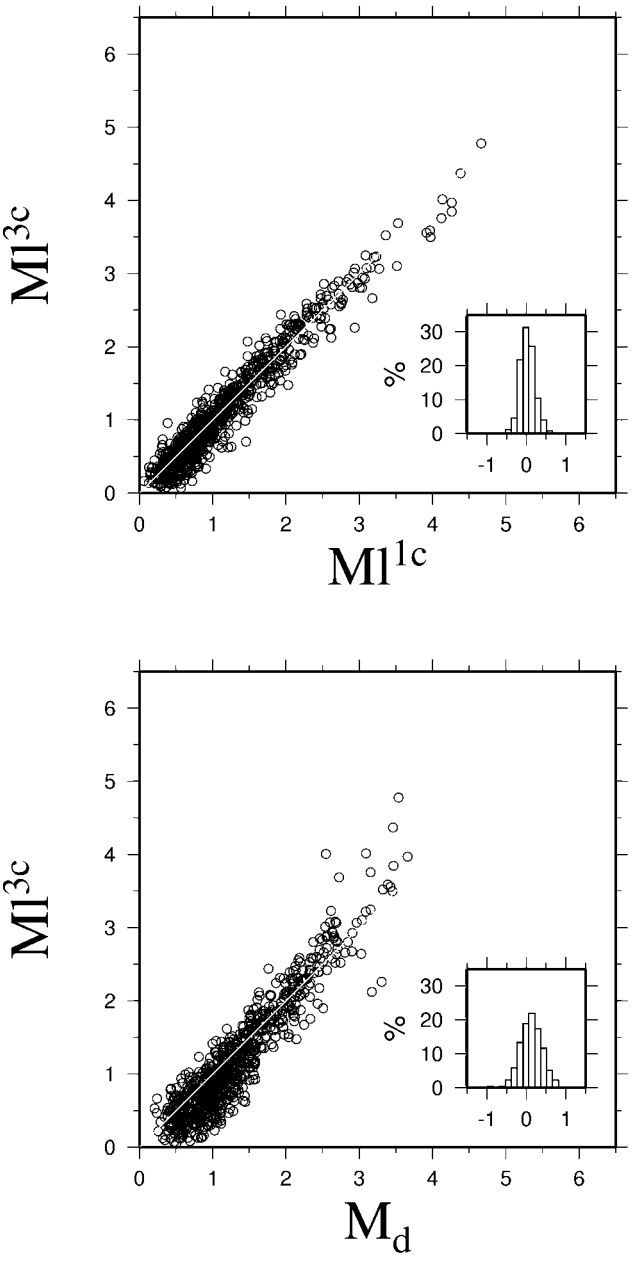

Figure 7. (top) Comparison between M_L^{3C} and M_L^{1C}. (bottom) Comparison between M_L^{3C} and M_D. The histograms of differences are shown inside each panel.

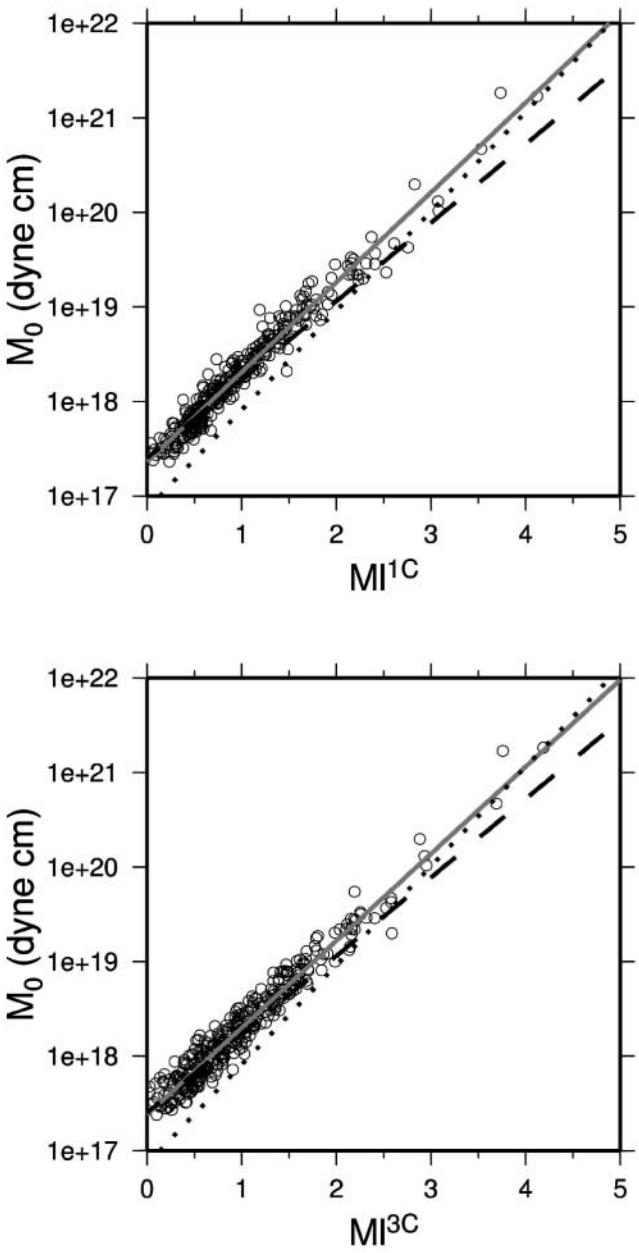

Figure 8. Seismic moment versus M_L^{1C} (top) and M_L^{3C} (bottom). The gray lines are the best least-squares fits and the dashed and dotted lines are the relationships valid for the northeastern Alps (Granet and Hoang Trong, 1980) and southwestern Germany (Sherbaum and Stoll, 1983), respectively.

Trong, 1980), whereas a better agreement with the results found for southwestern Germany (Sherbaum and Stoll, 1983) is observed at higher magnitudes (Fig. 8).

Conclusions

We developed magnitude calibration analysis in northwestern Italy by using three-component broad- or semibroadband stations and recordings from vertical short-period seismometers. The local magnitude scale computed using 10,057 synthetic Wood-Anderson maximum amplitudes (2822 earthquakes) from the horizontal components of the broad- or semibroadband sensors is:

$$M_L^{3C} = \log A + \log(R/100) + 0.0054(R - 100) + 3 - S$$

for magnitudes in the range $0 \leq M_L \leq 5$ and hypocentral distance R from 10 to 310 km. The station corrections S vary

from -0.13 to 0.57, assuming that S for the reference station STV2 is zero. The magnitudes M_L^{3C} predicted by this equation are used to calibrate scales based on either synthetic Wood-Anderson maximum amplitude (M_L^{1C} scale) or total signal duration (M_D scale), starting from vertical short-period recordings. The computed M_L^{1C} scale is

$$M_L^{1C} = \log A + \log(R/100) + 0.0041(R - 100) + 3 - S'$$

which we obtained by using the same reference site adopted for deriving M_L^{3C}.

The reliability of these scales has been assessed by comparing the predicted magnitudes with M_L^{3C}, using 827 earthquakes not included in the regression analysis. Although the M_L^{1C} and the M_L^{3C} scales showed good agreement over the range 0 to 5, the strategy adopted for evaluating the signal duration τ, that is, the selected corner frequencies of the bandpass filter and the threshold value assumed to determine τ, lead to reliable M_D only over the range 1 to 3. Because alternative strategies that allowed us to enlarge the range toward higher magnitudes always corresponded to an increase of the lower bound of the reliable magnitude range, in the present work, we adopted the settings that provided reliable duration magnitudes over the most sampled range of our dataset ($1 \leq M_D \leq 3$).

Considering the local magnitudes for the three component stations (M_L^{3C}) and those for the vertical, short-period stations (M_L^{1C}), the following seismic moment versus magnitude relationships have been derived for the western Alps:

$$\log M_0 = (0.92 \pm 0.01)\, M_L^{3C} + (17.38 \pm 0.08)$$
$$\log M_0 = (0.95 \pm 0.01)\, M_L^{1C} + (17.36 \pm 0.01)$$

The reliability of the obtained amplitude scale for the short-period network allows us to compile a seismic catalog including local magnitudes and seismic moments over the whole working period of the 1C network (from 1985 up today).

Acknowledgments

We thank P. Augliera for fruitful discussions and the staff of the RSNI network for their technical support. Suggestions from two anonymous reviewers strongly improved this article. The figures were drawn using the GMT software (Wessel and Smith, 1990). This research has been supported in part by Project GNDT2000-2002 coordinated by A. Amato and funded by Italian Civil Protection.

References

Bakun, W. H. (1984). Seismic moments, local magnitudes, and coda-duration magnitudes for earthquakes in central California, *Bull. Seism. Soc. Am.* **74,** 439–458.

Bakun, W. H., and W. B. Joyner (1984). The Ml scale in central California, *Bull. Seism. Soc. Am.* **74,** 1827–1843.

Baumbach, M., D. Bindi, H. Grosser, C. Milkereit, S. Parolai, R. J. Wang, S. Karakisa, S. Zünbül, and J. Zschau (2003) Ml scale in northwestern Turkey from 1999 Izmit aftershocks, *Bull. Seism. Soc. Am.* **93,** 2289–2295.

Ben-Zion, Y., and L. Zhu (2002). Potency-magnitude scaling relations for southern California earthquakes with $1.0 < \mathrm{Ml} < 7.0$, *Geophys. J. Int.* **148,** F1–F5.

Bormann, P. (2002). Magnitude of seismic events, in *IASPEI, New Manual of Seismological Observatory Practice*, P. Bormann (Editor), Vol. 1, GeoForschungsZentrum, Potsdam, 16–50.

Capponi, G., M. Cattaneo, and F. Merlanti (1985). The Ligurian earthquake of February 23, 1887, in *Atlas of Isoseismal Maps of Italian Earthquakes*, D. Postpischl (Editor), Vol. 114, 2A, CNR-PFG, Rome, 100–103.

Cattaneo, M., and P. Augliera (1990). The automatic phase picking and event location system at the IGG network, *Cah. Cent. Eur. Geodin. Seism.* **1,** 65–74.

Cattaneo, M., P. Augliera, S. Parolai, and D. Spallarossa (1999). Anomalously deep earthquakes in northwestern Italy, *J. Seism.* **3,** 421–435.

Cattaneo, M., P. Federici, and F. Merlanti (1981). L'uso della durata della registrazione come misura della magnitudo per terremoti vicini, C.N.R, Progetto Finalizzato Geodinamica: Seminario sulla magnitudo, Pubblicazione no. 481, (in Italian).

Efron, B. (1979). Bootstrap methods, another look at jacknife, *Ann. Stat.* **7,** 1–26.

Eva, E., S. Solarino, and D. Spallarossa (2001). Seismicity and crustal structure beneath the western Ligurian derived from local earthquake tomography, *Tectonophysics* **339,** 495–510.

Ferrari, G., V. Petrini, E. Patacca, and P. Scandone (1985). The Garfaguana earthquake of September 7, 1920, in *Atlas of Isoseismal Maps of Italian Earthquakes*, D. Postpischl (Editor), Vol. 114, 2A, CNR-PFG, Rome, 130–135.

Granet, M., and P. Hoang Trong (1980). Some medium properties at Friuli (Italy) from amplitude spectrum *Tectonophysics* **137,** 167–182.

Hanks, T. C., and D. M. Boore (1984). Moment-magnitude relations in theory and practice, *J. Geophys. Res.* **89,** 6229–6235.

Herrmann, R. B. (1975). The use of duration as a measure of seismic moment and magnitude, *Bull. Seism. Soc. Am.* **65,** 899–913.

Kanamori, H. (1983). Magnitude scale and quantification of earthquakes, *Tectonophysics* **93,** 185–199.

Langston, C. A., R. Brazer, A. A. Nyblade, and T. J. Owens (1998). Local magnitude scale and seismicity rate for Tanzania, east Africa, *Bull. Seism. Soc. Am.* **88,** 712–721.

Lee, W. H. K., and J. C. Lahr (1975). HYPO71 (revised): a computer program for determining hypocenter, magnitude, and first motion pattern of local earthquakes. *U.S. Geol. Surv. Open-File Rept. 75-311*, 100 pp.

Mayeda, K., A. Hofstetter, J. L. O'Boyle, and W. R. Walter (2003). Stable and transportable regional magnitudes based on coda-derived moment-rate spectra, *Bull. Seism. Soc. Am.* **93,** 224–239.

Morasca, P., K. Mayeda, L. Malagnini, and W. R. Walter (2005). Coda Derived Source Spectra, Moment Magnitudes, and Energy-Moment Scaling in the Western Alps, *Geophys. J. Int.* **160,** 263–275.

Paige, C. C., and M. A. Saunders (1982). LSQR: an algorithm for sparse linear equations and sparse least squares, *ACM Trans. Math. Soft.* **8,** 43–71.

Real, C. R., and T. L. Teng (1973). Local Richter magnitude and total signal duration in Southern California, *Bull. Seism. Soc. Am.* **63,** 1809.

Richter, C. F. (1935). An instrumental earthquake magnitude scale, *Bull. Seism. Soc. Am.* **25,** 1–31.

Richter, C. F. (1958). *Elementary Seismology*, W. H. Freeman and Co., San Francisco, 578 pp.

Scherbaum, F., and D. Stoll (1983). Source parameters and scaling laws of the 1978 Swabian Jura (southwest Germany) aftershocks, *Bull. Seism. Soc. Am.* **137,** 1321–1343.

Solarino, S., G. Ferretti, and C. Eva (2002). Seismicity of the Garfagnana-Lunigiana (Tuscany, Italy) as recorded by a network of semi-broad band instruments, *J. Seism.* **6,** 141–152

Solarino, S., E. Kissling, S. Sellami, F. Thouvenot, K. P. Bonjer, M. Granet, and G. Smeriglio (1997). Local earthquake catalog 1980 to 1995 of Alpine-Northern Apennine region for crustal seismic tomography, *Ann. Geofis.* **40,** 161–174.

Spallarossa, D., D. Bindi, P. Augliera, and M. Cattaneo (2002). An ML Scale in Northwestern Italy, *Bull. Seism. Soc. Am.* **90,** 1062–1081.

Spallarossa, D., G. Ferretti, P. Augliera, D. Bindi, and M. Cattaneo (2001). Reliability of earthquake location procedure in heterogeneous areas: synthetic tests in the South Western Alps, Italy, *Phys. Earth Planet. Int.* **123,** 247–266.

Uhrhammer, R. A., and E. R. Collins (1990). Synthesis of Wood-Anderson seismograms from broadband digital records, *Bull. Seism. Soc. Am.* **80,** 702–716.

Uhrhammer, R. A., S. J. Loper, and B. Romanowiez (1996). Determination of local magnitude using BDSN broadband records, *Bull. Seism. Soc. Am.* **86,** 1314–1330.

Wessel, P., and W. H. F. Smith (2000). *The Generic Mapping Tools (GMT)*, version 3.3.6, gmt.soest.hawaii.edu/gmt.html (last accessed October 2000).

Istituto Nazionale di Geofisica e Vulcanologia
via Bassini 15
20133 Milan, Italy
(D.B.)

DipTeRis, University of Genoa
Viale Benedetto XV, 5
16132, Genoa, Italy
(D.S., C.E.)

Istituto Nazionale di Geofisica e Vulcanologia
via di Vigna Murata 605
00143, Rome, Italy
(M.C.)

Manuscript received 24 May 2004.